González Martínez, AJ.; Moreno, M.; Barberá, J.; Conde Castellanos, PE.; Hernández Hernández, L.; Moliner Martínez, L.; Monzó Ferrer, JM.... (2013). Simulation study of resistor networks applied to an array of 256 SiPMs. IEEE Transactions on Nuclear Science. 60(2):592-598. doi:10.1109/TNS.2012.2226051.

Simulation study of resistor networks applied to an array of 256 SiPMs

Antonio J. González*, Manuel Moreno†, Julio Barberá ‡, Pablo Conde*, Liczandro Hernández*, Laura Moliner*, José M. Monzó*, Abel Orero*, Antonio Peiró *, Ramiro Polo ‡, Maria J. Rodriguez-Alvarez*, Ana Ros*, Filomeno Sánchez*, Antonio Soriano*, Luis F. Vidal*, José M. Benlloch*,
*Institute of Instrumentation for Molecular Imaging, Ciudad Politécnica de la Innovación, 46022 Valencia, SPAIN
Email: agonzalez@i3m.upv.es
†Instituto de Microelectrónica, 41092 Sevilla, SPAIN
‡Oncovision, Centro de Investigación Príncipe Felipe, 46012 Valencia, SPAIN

***Abstract*—In this work we describe a procedure to reduce the number of signals detected by an array of 256 Silicon Photomultipliers (SiPMs) using a resistor network to divide the signal charge into few readout channels. Several configurations were modeled, and the pulsed signal at the readout contacts were simulated. These simulation results were experimentally tested on a specifically designed and manufactured set of printed circuit boards. Three network configurations were modeled. The modeling provided encouraging results for all three configurations. The measurements on the prototypes constructed for this study, however, provided useful position-sensitivity for only one of the network configurations. The lack of input signal amplification into the networks, the SiPM dark current, as well as the complexity of an eight layers board with parasitic capacitances, could have caused the degradation of resolving the impact photon position. This is hard to overcome with external printed circuit boards and components.**

I. Introduction

Photosensors based on Silicon Photomultipliers (SiPMs) are considered good substitutes for the well established Photomultiplier Tube (PMT) technology [1], [2]. SiPMs are very fast, have high gain and they are almost unaffected by magnetic fields [3]. We intend to use arrays of SiPMs for the design of Positron Emission Tomography (PET) detectors compatible with Magnetic Resonance (MR) systems. To avoid the digitization of a considerable number of signals, multiplex circuits have been proposed. We are also interested in reducing the number of electronic components by avoiding the use of an amplifier for each SiPM.

SiPMs are also of great interest since they enable determination of the Time of Flight (TOF) of the 511 keV annihilation photons [4], are suitable for work under magnetic fields [3] and, are easy to manufacture when compared to PMTs. State–of–the–art whole body PET scanners based on PMTs can already provide TOF information to be considered during the data reconstruction process [5]. The proper use of SiPMs, meaning a satisfactory discrimination of signal time, could result on a time resolution in the order of few hundreds of picoseconds [6]. SiPMs exhibit their best performance in reduced active areas where the intrinsic dark counts (DC) are minimized. Moreover, the compatibility of these photosensors with magnetic fields suggests additional lines of research to develop hybrid PET-MR detectors.

We propose a detector block containing two main components, a SiPM array and a single monolithic crystal. The present design intends to use a crystal with a 50×50 mm^2 exit face, coupled to a matrix of 256 SiPMs each with an active area of 1×1 mm^2 (see Fig. 1). These types of detectors, in contrast to PMTs, account for moderate noise effects due to thermal excitation which is amplified and output as DC. Since SiPMs operate in Geiger mode, the DC contribution produces a continuous offset which contains fluctuations producing a baseline noise added to the pulse signals. Moreover, such DC significantly depends on the ambient temperature and the reverse bias voltage.

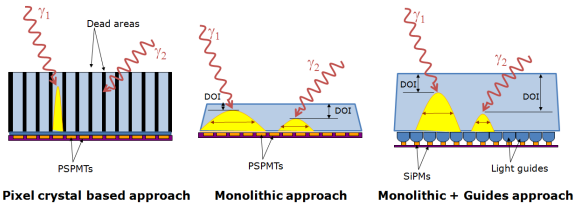

Fig. 1. Detector block approaches. From left to right, pixellated technology coupled to PSPMTs, monolithic crystal coupled to PSPMTs and monolithic crystal coupled to SiPM array via light guides.

Continuous scintillators allow one to determine the photon Depth of Interaction (DOI) without the need for additional components [7]. Crystals based on pixel arrays can provide discrete DOI information using multiple scintillation layers with different decay times [8], [9], but also continuous information when extra photosensors are located on opposite crystal faces [10]. Both methods inherently increase system complexity and cost. In contrast to these techniques, since monolithic crystals preserve the light distribution, the knowledge of the DOI can be obtained through the second moment, namely the light spread (see Fig. 1). Another important feature when dealing with continuous crystals is that their final spatial resolution is not limited by the pixel size as it is the case of crystal arrays, but rather by the determination of the center of gravity of the light distribution [11], [12].

We present a method to reduce the number of output SiPM signals based on different resistor network configurations. A

solution, based on signal charge sharing, has already been studied by various authors and served as a good approximation for most PMT tubes [13], but showing a complex output impedance for SiPMs. Recently, this configuration has been used for the readout of an array of SiPMs [14]. Reference [15] describes a similar work but using a Single Photon Avalanche Diodes (SPAD) model. As it will be described in the following section, a more convenient configuration for an array of SiPMs is one which avoids sharing the signal charge, see for instance references [16], [17].

In this work we have developed a complete model which describes the behavior of SiPMs. We have first modeled the response of a single SiPM including DC effects, after-pulsing and crosstalk, which are the statistical phenomena that affect their signal response. These effects have not been included in previous works [4] [18]. As will be described below, the design of certain resistor networks can overcome time and amplitude signal losses. Then, the presented SiPM model has been applied to an array of SiPM using various resistor network configurations. The simulation results will be further compared with real measurements.

II. Simulation study

The SiPM model, as well as the various resistor network configurations, were implemented in Verilog-A using a behavioral characterization. This description language -analog prolongation of Verilog HDL- allows us to obtain detailed models of semiconductor devices with high level of abstraction. Moreover, it is important to consider that many accepted simulation packages permit behavioral simulations in different situations, so the model can be used in simulation tools like SPECTRE, that was our case.

A. SiPM model

Since SiPMs are based on Avalanche Photodiodes (APDs) working in Geiger mode along with quenching circuits, macroscopic currents generated by individual photons can be detected. Indeed, SiPMs can be seen as the combined work of isolated SPADs. From such a point of view, one considers that the parallel effort of 10^2-10^5 SPADs working under a passive quenching circuit defines the term SiPM [19]. The SiPMs output pulse is similar to that of the SPADs and proportional to the number of those triggered (analog sum of the individual current of cells [20] [21]).

There are three factors that characterize these devices, namely the internal noise, the dead time and the temperature of operation. In the following, we will further describe these effects since they are to be considered in the proposed SiPM model.

The internal noise is often dominated by the dark counts, which as commented above are produced by photon generated carriers and thermally generated dark current carriers. However, the afterpulses and the crosstalk effect also contribute to this noise. The afterpulses are spurious pulses following the true signal, which occur when the generated carriers are trapped by crystal (Si) defects and then released with a certain time delay. During the avalanche process in Silicon, light is produced at a probability of around 10^{-5} photons/electron [22]. The crosstalk effect arises since, despite the very low number of generated secondary photons, they can still be captured by neighboring cells, which can then be triggered to fire as well.

During the modeling of the SiPM, several temporal parameters have to be considered. The quenching time is the elapsed time between the trigger of the avalanche current and its extinction. The recharge (or reset) time is the time between the quenching of the avalanche and the return to the initial conditions of bias. While the element is recharging, the detection efficiency and gain are lower than normal, but the element can be retriggered during the recharge time. This minimum time elapsed for the detection of two consecutive photon arrivals is the dead time.

Finally, temperature affects the behavior of the SiPMs considerably and has to be modeled carefully for a proper characterization of the device. Important parameters such as the breakdown voltage, the carrier generation rate or the lifetime of internal levels strongly depend on the temperature [23].

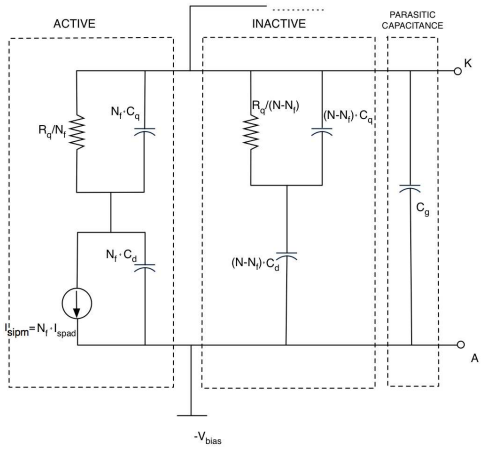

Fig. 2. Equivalent circuit of the SiPM, containing the capacitance of the diode C_D and a current source which emulates the current flowing through it (depends on its equivalent resistance, R_D, see Eq. 1), the quenching resistor R_q and its parasitic capacitance associated C_q, as well as the grid parasitic capacitance C_g.

In particular we have modeled the SiPM of Hamamatsu Photonics, so-called MPPC (Multi-Pixel Photon Counter), with a 1×1 mm^2 active area and 50×50 μm^2 cells, corresponding to the model S10362-11-50C [24].

The model normally used to describe a SiPM is shown in Figure 2. It is based on the models presented in [4] [18] [25] in which the equations and measurements needed for characterizing these devices are extensively explained. This model consists of an active part due to the cells that are fired (N_f), a passive one with the inactive cells ($N-N_f$) -each with the quenching resistance, the emulation of the current through the device and the corresponding parasitics- and an overall parasitic capacitance stemming from the fabrication process.

The parameter values used in this work are the following: R_q=175 kΩ, C_q=5 fF, C_D=25 fF, C_g=30 fF and N_{tot}=400.

However, this model has some problems. First of all, experimental results show that the current flowing through the SPADs is linearly dependent on the bias voltage only if this current is higher than a certain level called latching current [26] [27]. If not, the current will no longer be self-sustained. A more realistic description would require the use of a piecewise linear characteristic [26], though convergence problems due to discontinuity during the simulations when changing from one region to another suggest the use of a straight line in describing the behavior of the SiPM in the avalanche region. In this work we modeled the current ($I_{SiPM} \equiv I$) through the device as [23]:

$$I = \begin{cases} I_S & V_D < V_{BR} \\ N_f \cdot (I_S + \frac{V_n}{R_D} ln(1 + e^{\frac{V_D - V_{BR}}{V_n}})) & V_D > V_{BR} \end{cases} \quad (1)$$

where I_S is the saturation current, R_D is the internal resistance, V_n is a normalization voltage, V_{BR} is the breakdown voltage and V_D is the voltage applied to the device. The fit parameters were I_S=1.07×10^{-17} A, V_n=10 mV, R_D=1 kΩ and V_{BR}=71.2 V.

The model is incomplete, due to the exclusion of statistical phenomena which are key when characterizing the SiPMs. The turn-on of the device is defined as the moment when a photon striking the surface of a SiPM has a certain probability of being detected and consequently, generating an avalanche current [28].

This probability is given by the photon detection efficiency (PDE), which varies depending on the wavelength of the incoming photons. Nevertheless, the avalanche current could also originate in non-desired phenomena: the dark count, afterpulsing and crosstalk events. The latter two are included in the photon detection efficiency as stated in the datasheet provided by the manufacturer [24]. In the case of the dark counts, they are modeled as in [23], adapting the values of the parameters to those specified by the manufacturer.

Turn-off of the device is modeled by defining the latching current as a threshold value below which the avalanche current is no longer self-sustained. Typical values for this current are in the order of 40-120 μA for the SPADs [29]. Once the model has been implemented, it is necessary to test its validity. For that purpose, the circuit proposed by the manufacturer in the datasheet of the product was built [24]. This allowed us to perform experimental measurements and compare them with the simulation results.

This circuit comprises an input resistance of 10 kΩ which limits the amount of current flowing through the SiPM. A 50 Ω resistance was connected to the anode device to sense the output signal of the SiPM. In addition to this resistor, a 100 nF capacitor was added as well as a voltage source for biasing the device slightly above its breakdown voltage.

Figure 3 depicts the modeled curve at the anode of the SiPM after the arrival of a photon. The concordance of this result (both in the amplitude and width of the peak) with known data [3] [30] shows the effectiveness of the developed model. This model is extensible to other SiPM designs and it is only necessary to perform the measurements described in the bibliography [18] [31] to obtain the particular values of the figures of merit that characterize the behavior of the detector.

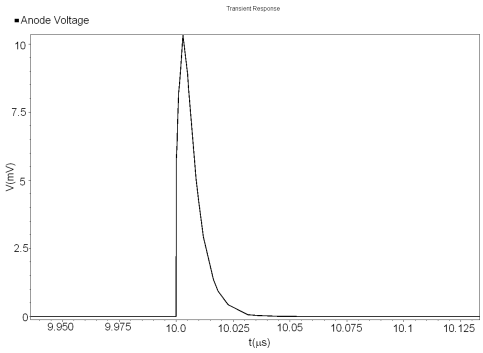

Fig. 3. Modeled signal obtained for a single SiPM.

B. Resistor networks

Once we have successfully modeled a single SiPM device, we studied SiPM matrices coupled to different readout configurations. In this work we have focused on several resistance networks which are described in the following subsections as alternatives for reading the detector matrices. We have performed simulations using the model developed previously for the SiPMs with the aim of reproducing the experimental results. The electronic simulations have been carried out with Spectre, in the Virtuoso environment by Cadence.

1) Discretized Positioning Circuit: The first resistive network we simulated consists of a serial connection of all the resistors. Such a network is represented in Figure 4 and it is called Discretized Positioning Circuit (DPC). Of the three possible readout techniques that we will study, it is that which has been applied longest. In particular, it has been successfully utilized when reading position sensitive photomultiplier tubes (PSPMTs) [13] but also with an array of SiPMs [14]. See also references [32], [33] for gamma camera applications with PSPMTs. It is the simplest topology amongst those studied in this work. Through an $I - V$ conversion, it is possible to measure the voltage at the four corner outputs of the network. With this type of configuration, the planar (XY) impact positions, are obtained through the so-called Anger logic [34], [13].

$$\begin{aligned} X_{position} &= \frac{V_A + V_B - V_C - V_D}{V_A + V_B + V_C + V_D} \\ Y_{position} &= \frac{V_A - V_B - V_C + V_D}{V_A + V_B + V_C + V_D} \end{aligned} \quad (2)$$

The analyses carried out have been transient simulations in which we have emulated the arrival of photons to a 8×8 matrix of SiPMs (from left to right, and from top to bottom, Fig. 4). This network has shown attenuation problems in prior studies, especially for rows and columns in the middle of the

matrix. Moreover, delays in the arrival of the different signals due to the various paths traveled depending on the position of the impact have been observed [34].

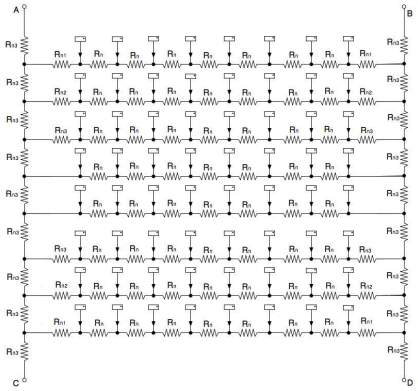

Fig. 4. Schematic of the DPC resistor network.

Figure 5 shows the results of a transient analysis. We selected an array of 64 elements due to its similarity with the multi-anode structure of most PSPMTs. On left hand side we plot the resulting V_A and V_D signals. V_B and V_C have a complementary behavior. The map on the right side of the figure, depicts the X and Y positions after applying Eq. 2 to the obtained data. The yellow dots represent the ideal positions of the SiPM matrix. It is clear that, except for the points in the edges, there is a distortion in the positions of the matrix and the separation between the different elements is insignificant, so this network presents a bad spatial resolution. Moreover, for the intermediate rows and columns the attenuation is so important that the signals are, in practice, hardly detectable. This problem can be limited by changing the sensing resistance connected to ground, though this was not enough in order to obtain useful signals. It seems that, despite the simplicity of this topology and its suitability in the case of PMTs, in the current simulation study (R_n=1kΩ, R_{n1}=600Ω, R_{n2}=300Ω and R_{n3}==100Ω), it is not the most appropriate for the readout of an array consisting of a large number of SiPM devices.

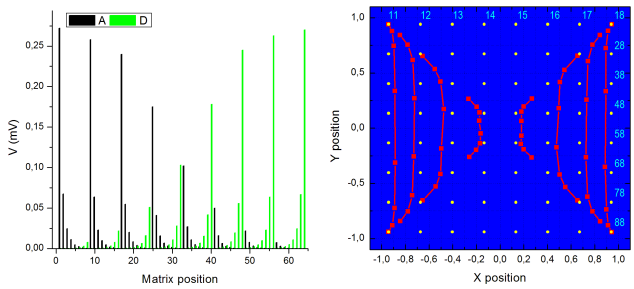

Fig. 5. Results for the DPC circuit for an 8×8 SiPM array. The left plot shows the V_A in black and the V_D in green colour, respectively. The map on the right side indicates in red squares the return X and Y positions calculated using Eq. 2. Here, the yellow dots indicate the ideal SiPM location.

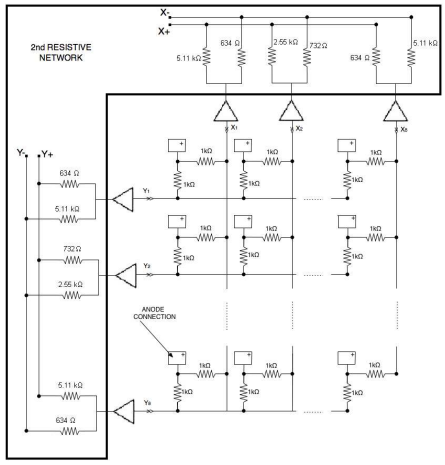

Fig. 6. Schematic of the SCD resistor network.

2) Symmetric Charge Division Circuit: The alternative approach for adding up the entire charge into a large resistive division network, is to divide the charge into an X and Y decoder network. This method has already be suggested for both PSPMT [16], [35] and SiPM arrays [17] with satisfactory results. The incoming charge is shared in two parts (there is an equitable division of charge), one part collects the signals for X, and the other part those for Y. Figure 6 also shows a schematic example for 8×8 input signals. This technique is referred to as Symmetric Charge Division (SCD). In order to obtain the final XY impact position a signal multiplexing is still required [36], as the first network does not allow us to discriminate the impact position of the photon and it would be appropriate to reduce the number of signals. Equation 3 shows how these coordinates are recovered. In this approach each row and column signal output needs to be pre-amplified before the next multiplexing.

$$X_{position} = \frac{X_+ - X_-}{X_+ + X_-}, \quad Y_{position} = \frac{Y_+ - Y_-}{Y_+ + Y_-} \tag{3}$$

where X_+, X_-, Y_+ and Y_- refer to the up and down signal corners (see Fig. 6) [33].

With this resistor configuration, we simulated an array of 8×8 SiPMs. The analysis carried out was the same as in the previous section for the DPC, after a proper choice of the resistances [33]. We included the charge division circuit as well as several other components of the expected board. The results for X_+, X_-, Y_+ and Y_- look very promising since the steps on the different rows and columns were well separated. Figure 7 depicts a portion of the results for the 8×8 SiPM array in which it can be observed that steps of close to 0.25 mV were achieved in between neighboring channels in both the X and Y directions. When comparing these results with the DPC approach we observe that the attenuation drawback in centered impacts has been suppressed. On the right hand side of Figure 7 we show a map with the X and Y positions obtained after applying Eq. 3 to the data for X_+, X_-, Y_+ and Y_-. We

observe an almost negligible distortion on the return SiPM position making it possible to accurately resolve the impact position.

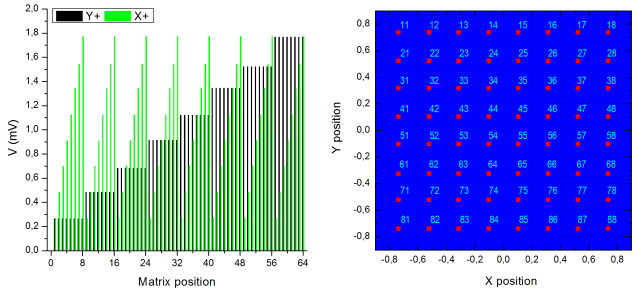

Fig. 7. Results for the SCD circuit for an 8×8 SiPM array. The left plot shows the X_+ in black and the Y_+ in green colour, respectively. The X_- and Y_- behave inversely. The map on the right indicates the return X and Y positions calculated using Eq. 3.

This approach contains two resistor networks, one for the X and one for the Y direction. In addition to these, we included a third based on the same connection principle but with lower resistances to be used for the time discrimination of the incoming event. Since this trigger signal is obtained by feeding all output signals into an operational sum, most possible delay losses should be reduced.

Although in this case the attenuation problems seem to vanish and it presents a good spatial resolution, a drawback related to scalability appears, being that a change in the dimensions of the matrix of SiPMs would imply a redesign of the second multiplexing circuit (X_+, X_-, Y_+ and Y_-).

3) Weighted Charge Division Circuit: Following the topology of the prior SCD circuit we introduced an additional variable with the aim of avoiding the second multiplexing circuit and the required number of pre-amplifiers scaling with the number of detectors. This variable is intended to use resistances with increasing values from one row or column to the next. These values are chosen in a similar way as it was performed for the second network of the SCD circuit [33]. The schematic of this design is shown in Figure 8. The output signal of all detectors, after passing through a sum operational, should directly return a value proportional (weighted) to the conductance of the resistor placed in a particular X and Y photon impact coordinate. Thus, we dubbed this circuit Weighted Charge Division (WCD). However, this topology presents a disadvantage with regards to the case of the SCD. As can be seen in Figure 8, there is a variation for a given row of the resistance values connected to the X coordinate. This means that the Y signal will change depending on the column in which the hit occurs, although the photon reaches the same row (the same applies for X when dealing with the same column). For this reason, the bias resistance to ground (200 Ω, 10% of the value of the smallest resistance in the network) has been chosen in such a way that it becomes the dominant impedance and, thus, the current is only slightly influenced by the resistances connected to X and Y. With

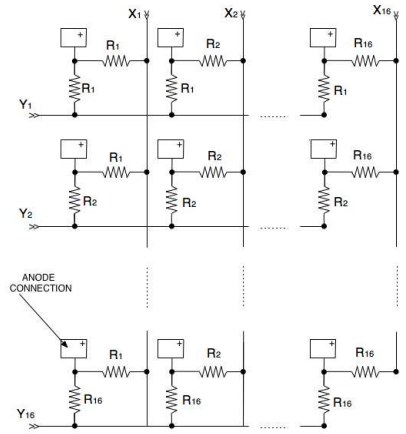

Fig. 8. Schematic of the WCD resistor network. R_1, R_2,... R_{16} stand for resistors with increasing values. In our case the values in kΩ are 2, 2.2, 2.4, 2.7, 3, 3.3, 3.9, 4.7, 5.6, 6.8, 8.2, 10, 12, 16, 22 and 30, respectively.

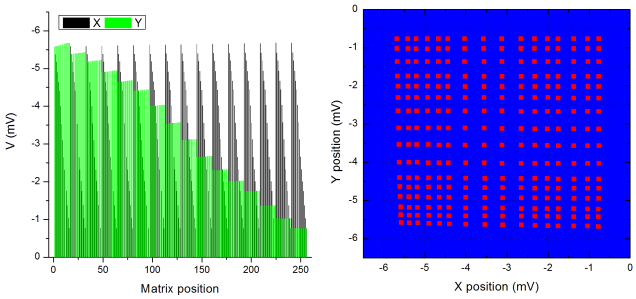

Fig. 9. Results for the WCD circuit for a 16×16 SiPM array. The left plot shows the X and Y components in black and green colours, respectively. The right plot depicts the bidimensional map of X and Y positions.

this, we fulfill our goal of obtaining approximately the same signal in $X(Y)$ for photons hitting the same column (row). The value of this resistor allows for measurable signals after amplification. When selecting the ground resistor, there must be a compromise between good working behavior of the X and Y networks and a reduction of signal attenuation causing the need of high amplification. A low input impedance of the amplifiers is required in order to avoid X-Y crosstalk or non-proportional charge division. The results for the WCD for a SiPM array of 16×16 units are shown in Figure 9. An array of 256 elements was directly selected since there are no previous and comparable results based on this configuration.

We observed that the WCD returns in some cases closer values of adjoining input signals than the SCD, with a minimum value of 0.15 mV, as can be seen, for instance, in the Y plot in Figure 9. This is due to the greater dimension of the matrix in the WCD case (16×16) compared to the SCD case (8×8). This means that the greater the dimension of the matrix, the more difficult it becomes to choose the values of the resistances, the higher the system resolution necessary for discriminating differences that could be in the range of only few mV. Figure 9 also depicts a two dimensional map of the X

and Y values. In contrast to the SCD map, we observe a slight distortion of the SiPM positions but with enough resolution to determine any detector location. As was done for the SCD circuit, we also included here an additional resistor network to provide us with time and triggering signal.

Summarizing, the simulation results for the WCD avoid the attenuation of signals produced for impacts occurring in the centered region. All SiPM positions are clearly resolved. Moreover, in contrast to the DPC or the second resistive network for SCD methods, there is no need for further multiplexation of the signals, and there are not time differences depending on the impact position.

III. Experimental Results

The simulation results obtained with the DPC approach show a tendency similar to the preliminary measurements carried out with an array of 8×8 SiPM devices (S10362-11-050 from Hamamatsu). We used a LYSO scintillation crystal with a trapezoidal shape [11] [12] having an exit face of 50×50 mm^2 and a thickness of 10 mm. The area covered by the SiPM array was however, that of close to about 25×25 mm^2, the active area being only 8×8 mm^2. The coupling between the scintillator and the photo-sensors was directly performed by means of optical grease. Although not implemented in this work, a more efficient coupling method using optical devices has been extensively studied elsewhere [12]. In Figure 10 there is a photograph of the scintillator crystal and the pack of PCB boards. The board placed directly below the crystal contains the SiPM array. The 2D plot on the left hand side depicts the XY map obtained with the DPC approach. These data were acquired with no radioactive source, and only background events were recorded. The bias voltage to the SiPM array was 71 V for an acquisition time of 60 s. The depletion effect in the central region caused by the signal attenuation can be easily observed, as it was also obtained by simulation (see also the depletion effect in Fig. 5 left).

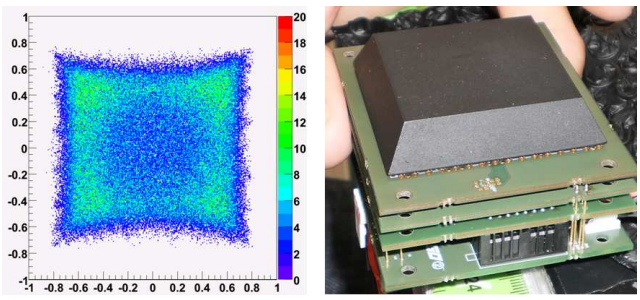

Fig. 10. Left, 2D contour plot of background activity obtained with the DPC approach. The axes represent the X and Y impact coordinates. Right, LYSO crystal mounted on top of the PCBs containing the SiPMs array and associated electronic.

Instead of testing both the SCD and the WCD approaches we decided to only test the WCD since the expected results would be more convenient than the SCD in terms of avoiding extra multiplexing and amplification components. The manufactured PCB placing the 3 resistor networks (2 for the XY positions and one for the energy/time) contained 8 layers and the resistors had a size of 1×0.5 mm^2 with tolerances below 1%. The SiPM array used in these measurements was identical to that described above for the DPC approach. However, in order to more efficiently couple the crystal we used a smaller LYSO unit of 32×32 mm^2 entrance and exit faces, and a thickness of 18 mm (see Fig. 11).

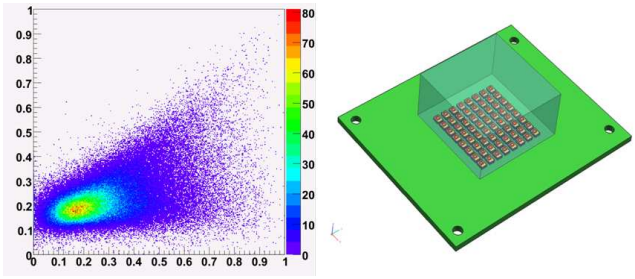

Fig. 11. Left, 2D contour map for a uniform background using the WCD circuit. Right, sketch of the crystal and SiPM array coupling used for the tests with the WCD circuit.

The results of the WCD measurements showed a strong concentration of data in a very small region (Fig. 11), very distinct from the observed image with the DPC attenuated data. By injecting signals point by point with a function generator (resembling that of the LYSO profile type), the results in X and Y position varied accordingly to the simulation. However, when two or more signals were injected into the WCD circuit, the image shown in Figure 11 appeared. It seems that the PCB design accounts for significant coupling effects of the two X and Y resistor networks. We also performed measurements by lowering the common resistance of the trigger resistor network to avoid extra coupling with this signal without success.

IV. Conclusion

In this work we have described several methods to reduce the readout channels of an array of SiPM detectors. This type of photosensors are the subject of much interest for high energy physics, and medical applications, among others. However, the number of channels to be processed tends to increase when higher performance of the devices is required. Thus we deem a multiplexation or reduction of signals to be the proper course.

We utilized the existing and widely used DPC resistor network with slight modifications for use on SiPM arrays. We successfully modeled the performance of a single SiPM using the Verilog-A language. We extended this task and simulated the DPC approach observing a satisfactory qualitative concordance between the real and simulated data, as can be observed in the depletion effect shown in Figures 5 and 10.

The extension of this model to an approach in which the signal attenuation drawbacks were suppressed, was also performed. Here, two different configurations were studied; the SCD and the WCD. The simulation of both resistor networks suggested promising results when SiPM input signals were fed into the system. The WCD was especially examined for an array of 16×16 SiPMs since it could directly provide the X

and Y impact position without further multiplexing. Moreover, both models also solved delay time problems observed for the DPC. However, when this model was put into the practice, the results showed a poor resolving power for planar XY coordinates. An *a priori* analysis of the results suggest a coupling effect of the X and Y signals due to capacitances in the PCB board.

ACKNOWLEDGMENT

This work was supported by the Spanish Plan Nacional de Investigación Científica, Desarrollo e Innovación Tecnológica (I+D+I) under Grant No. FIS2010-21216-CO2-01, the Valencian Local Government under Grant PROMETEO 2008/114 and through the JAE-Predoc grant from CSIC (BOE 29/01/2010).

REFERENCES

[1] S. Moehrs, A.D. Guerra, D.J. Herbert and M.A. Mandelkern, *A detector head design for small-animal PET with silicon photomultipliers (SiPM)*, Phys. Med. Biol. **51** 1113 (2006).

[2] D.R. Schaart, H.T. van Dam, S. Seifert, R. Vinke, P. Dendooeven, H. Löhner and F.J. Beekman, *A novel, SiPM-array-based, monolithic sicntillator detector for PET*, Phys. Med. Biol. **54** 3501 (2009).

[3] S. España, L.M. Fraile, J.L. Herraiz, J.M. Udías, M. Desco and J.J. Vaquero, *Performance evaluation of SiPM photodetectors for PET imaging in the presence of magnetic fields*, Nucl. Instrum. Meth. A **613** 308 (2010).

[4] S. Seifert, D.R. Schaart, H.T. van Dam, J. Huizenga, R. Vinke, P. Dendooven, H. Lohner and F.J. Beekman, *A High Bandwidth Preamplifier for SiPM-Based TOF PET Scintillation Detectors*, IEEE Nucl. Sci. Symp. Conf. Rec. **NM1-2** 1616 (2008).

[5] H. Zaidi, N. Ojha, M. Morich, J. Griesmer, Z. Hu, P. Maniawski, O. Ratib, D. Izquierdo-Garcia, Z.A. Fayad and L. Shao, *Design and performance evaluation of a whole-body Ingenuity TF PETMRI system*, Med. Phys. Biol. **56** 3091 (2011).

[6] P. Buzhan, B. Dolgoshein, E. Garutti, M. Groll, A. Karakash, V. Kaplin, V. Kantserov, F. Kayumov, S. Klyomin, N. Kondratiev, A. Pleshko, E. Popova, F. Sefkow, *Timing by silicon photomultiplier: A possible application for TOF measurements*, Nucl. Instrum. Meth. A **567** 353 (2006).

[7] C. Lerche, J. Benlloch, F. Sanchez, N. Pavon, B. Escat, E. Gimenez, M. Fernandez, I. Torres, M. Gimenez, A. Sebastia and J. Martinez, *Depth of gamma-ray interaction within continuous crystals from the width of its scintillation light-distribution*, IEEE Trans. Nucl. Sci. **52** 560 (2005).

[8] J. Jung, Y. Choi, Y. Chung, O. Devroede, M. Krieguer, P. Brunyndonckx and S. Tavernier, *Optimization of LSO/LuYAP phoswich detector for small animal PET*, Nucl. Instrum. Meth. A **571** 669 (2007).

[9] U. Heinrichs, U. Piertrzyk and K. Ziemons, *Design optimization of the PMT-ClearPET prototypes based on simulation studies with GEANT3*, IEEE Trans. Nucl. Sci. **50** 1428 (2003).

[10] W.W. Moses and S.E. Derenzo, *Design studies for a PET detector module using a PIN photodiode to measure depth of interaction*, IEEE Trans. Nucl. Sci. **41** 1441 (1994).

[11] J.M. Benlloch, V. Carrilero, A.J. González, J. Catret, Ch.W. Lerche, D. Abellán, F. García de Quirós, M. Giménez, J. Modia, F. Sáncheza, N. Pavón, A. Ros, J. Martínez, A. Sebastiá, *Scanner calibration of a small animal PET camera based on continuous LSO crystals and flat panel PSPMTs*, Nucl. Instrum. Meth. A **571** 26 (2007).

[12] A.J. González Martínez, A. Peiró Cloquell, F. Sánchez Martínez, L.F. Vidal San Sebastian and J.M. Benlloch Baviera, *Innovative PET detector concept based on SiPMs and continuous crystals*, Nucl. Instrum. Meth. A, *DOI:10.1016/j.nima.2011.11.029* (2011).

[13] S.R. Cherry, Y. Shao, S.B. Siegel, and R.W. Silverman, *High Resolution Detector Array For Gamma-ray Imaging*, US Patent 5719400 (1998).

[14] P. Dokhale, C. Stapels, J. Christian, Y. Yang, S. Cherry, W. Moses, and K. Shah, *Performance Measurements of a SSPM-LYSO-SSPM Detector Module For Small Animal Positron Emission Tomography*, IEEE Nucl. Scien. Sympos. Conf. Record, 2809 (2009).

[15] K. Iniewski, *Biological and Medical Sensor Technologies*, CRC Press (Taylor & Francis Group), Boca Raton, (2012), ISBN:978-1-4398-8267-3.

[16] V. Popov, *Matrix output device readout system*, US Patent 6747263 B1 (2004).

[17] S. Majewski, J. Proffitt, A. Stolin, and R. Raylman *Development of a Resistive Readout for SiPM Arrays*, 2011 IEEE Nucl. Scien. Sympos. Conf. Record, 3939 (2011).

[18] F. Corsi, A. Dragone, C. Marzocca, A. Del Guerra, P. Delizia, N. Dinu, C. Piemonte, M. Boscardin and G.F. Dalla, *Modelling a silicon photomultiplier (SiPM) as a signal source for optimum front-end design*, Nucl. Instrum. Meth. A **572** 416 (2007).

[19] H. van Dam, S. Seifert, R. Vinke, P. Dendooven, H. Lohner, F.J. Beekman and D.R. Schaart, *A Comprehensive Model of the Response of Silicon Photomultipliers*, IEEE Trans. Nucl. Scien. **57** 2254 (2010).

[20] L.H.C. Braga, L. Pancheri, L. Gasparini, R.K. Handerson and D. Stoppa, *A mini-SiPM array for PET detectors implemented in a 0.35-um HV CMOS technology*, IEEE (PRIME, Ph.D. Research in Microelectronics and Electronics) 181 (2011).

[21] T. Frach, G. Prescher, C. Degenhardt and B. Zwaans, *The digital silicon photomultiplier System architecture and performance evaluation*, IEEE Nucl. Scien. Sympos. Conf. Record, 1722 (2010).

[22] A. L. Lacaita, F. Zappa, S. Bigliardi and M. Manfredi, *On the Bremsstrahlung Origin of Hot-Carrier-Induced Photons in Silicon Devices*, IEEE Trans. Electron Devices **40** 577 (1993).

[23] G. Giustolisi, R. Mita and G. PAlumbo, *Behavioral modeling of statistical phenomena of single-photon avalanche diodes*, Int. J. Circ. Theor. Appl., *DOI:10.1002/cta.748* (2011).

[24] *www.hamamatsu.com*

[25] K.A. Wangerin, G. Wang, C. Kim and V. Danon, *Passive Electrical Model of Silicon Photomultipliers*, IEEE Nucl. Sci. Symp. Conf. Rec. **M10-202** 4906 (2008).

[26] F. Zappa, A. Tosi, A. Dalla and S. Tisa, *SPICE modeling of single photon avalanche diodes*, Sensors and Actuators A **153** 197 (2009).

[27] S. Tisa, F. Zappa, A. Tosi and S Cova, *Electronics for single photon avalanche diode arrays*, Sensors and Actuators A **140** 113 (2007).

[28] A. Rochas, M. Gosch, A. Serov, P.A. Besse, R.S. Popovic, T. Lasser and R. Rigler, *First fully integrated 2-D array of single-photon detectors in standard CMOS technology*, IEEE Photonics Technology Letters **15** 963 (2003).

[29] R. Mita, G. Palumbo and P.G. Fallica, *Accurate model for single-photon avalanche diodes*, IET Circuits Devices Syst. **2** 207 (2008).

[30] D. Renker, *Geiger-mode avalanche photodiodes, history, properties and problems*, Nucl. Instrum. Meth. A **567** 48 (2006).

[31] I. Rech, A. Ingargiola, R. Spinelli, I. Labanca, S. Marangoni, M. Ghioni and S. Cova, *Optical crosstalk in single photon avalanche diode arrays: a new complete model*, Optics Express **16** 8381 (2008).

[32] F. Sánchez, J.M. Benlloch, B. Escat, N. Pavón, E. Porras, D. Kadi-Hanifi and J.A. Ruiz, *Design and tests of a portable mini gamma camera*, Med. Phys. **31** 1384 (2004).

[33] P.D. Olcott, J.A. Talcott, C.S. Levin, F. Habte, and A.M.K. Foudray, *Compact Readout Electronics for Position Sensitive Photomultiplier Tubes*, IEEE Trans. Nucl. Scien. **52** 21 (2005).

[34] S. Siegel, R.W. Silverman, Y. Shao, and S.R. Cherry, *Simple charge division readouts for imaging scintillator arrays using a multi-channel PMT*, IEEE Trans. Nucl. Scien. **43** 1634 (1996).

[35] V. Popov, S. Majewski and A.G. Weisenberger, *Readout Electronics for Multianode Photomultiplier Tubes With Pad Matrix Anode Layout*, 2003 IEEE Nucl. Scien. Sympos. Conf. Record, 2156 (2004).

[36] V. Popov, S. Majewski, A.G. Weisenberger, and R. Wojcik *Analog Readout System with Charge Division Type Output*, 2001 IEEE Nucl. Scien. Sympos. Conf. Record, 1937 (2002).